RSC Advances

Journal Name

RSC Advances

ARTICLE TYPE

Solar-Assisted Dual Chamber Microbial Fuel Cell with CuInS$_2$ Photocathode

Siwen Wang, Xiaoling Yang,* Yihua Zhu,* Yunhe Su and Chunzhong Li

We report a solar-assisted microbial fuel cell (solar MFC) that can produce electricity through coupling the microbial anode with flower-like CuInS$_2$ (CIS) as photocathode. Scanning electron microscopy images displayed hierarchical structure of CIS, which would be beneficial to facilitate the electron transfer in MFC performance. The electrochemical and photo-responsive activity of CIS was investigated

₁₀ with cyclic voltammetry, linear sweep voltammetry (LSV) and photocurrent tests. We proposed the hypothesized mechanism of MFC operation was that light-responsive CIS generated electron-hole pairs and triggered bioanode for electricity generation. LSV curves and photocurrent data displayed that flower-like CIS showed enhanced photocurrent generation under visible light irradiation. Based on the improved photoelectrochemical properties, the solar MFC achieved maximum power density of 0.108

₁₅ mW cm^{-2}, and current density of 0.62 mA cm^{-2}. CIS as photocathode presented comparable power density with Pt/C in MFC.

1. Introduction

Development of new energy solutions with minimum impact on the environment is critical as the supply of fossil fuels decrease
₂₀ and the environmental problems intensify recent years. In this regard, microbial fuel cells (MFCs) hold great potential to address both issues simultaneously, by converting chemical energy stored in biodegradable organic matter directly into electricity energy.[1-4] However, at the present stage, wide
₂₅ application of this technology is not straightforward because it's a costly and energy-consuming process.[5] The cathode limitation is currently considered as the major limiting factor to reduce the device cost and achieve a high electricity output.[6,7] Considerable efforts have been made on optimization of MFC design of
₃₀ cathodes and catalysts to deal with the poor oxygen reduction rate during oxygen reduction reaction (ORR),[8] or the high internal resistance of cathode materials,[9] and the high cathodic overpotential.[10,11] There are many reports on cathode materials, such as Platinum (Pt)-loaded carbon cloth or carbon paper,[12-14]
₃₅ conductive polymer coated stainless steel mesh,[15] nano-structured MnO$_X$ electrodeposited carbon paper [16]and multi-walled carbon nanotube composite modified carbon cloth.[17]

In addition to electrochemical methods, efficient electricity generation can also be achieved by incorporating an external
₄₀ required source, such as solar energy, to facilitate electron transfer with an extra driven force.[18] This has led to the development of photocathode by employing semiconductors, which assist the cathodic electrocatalytic reactions in reaction process. With respect to photocatalytic reactions, electron-hole
₄₅ pairs are generated at a semiconductor upon photo irradiation, then the photogenerated holes in valance band (VB) are

transferred to a catalytically active site for redox reactions, meanwhile photogenerated electrons in the conducton band (CB) are delivered from the anode to reduce electron acceptors in the
₅₀ surface of cathode.[19] So far, several semiconductors have been used for cathodic catalysis in MFCs. Among these, TiO$_2$[19,20] and Cu$_2$O[21,22] have been used as an efficient photoelectrocatalyst in cathode reaction. However, due to a relative wide band gap, TiO$_2$ suffers from lower quantum efficiency and photocatalytic
₅₅ performance. Cu$_2$O suffers from poor stability due to photocorrosion.[23] Therefore, designing a cost-effective and sustainable cathode material is crucial and urgent to the development and scale-up of MFCs.

Recent photoelectrochemical application has tended to ternary
₆₀ chalcopyrites CuME$_2$ (M = Ga, In; E = S, Se, Te) type semiconductors, which have been considered as potentially less toxic materials. Among the numerous CuME$_2$ compounds, CuInS$_2$ (CIS) has been well studied in consequence of its suitable bandgap for light-harvesting applications. Therefore, CIS
₆₅ with different morphology has presented excellent light absorption properties in solar cells,[24,25] photocatalysis of hydrogen generation,[26] and optical detection of biological molecules.[27,28] Based on above advantages, CIS could be capable for solar energy conversion in cathode reaction of MFCs.

₇₀ Developing well-controlled morphology of the photocatalysts may furnish us with a promising way for improving the cathode performance. Hierarchical structured porous materials would provide dispersion of active sites and allow easy transmission of light, which have been involved in newly developed energy
₇₅ storage and conversion systems.[18,29] Among many kinds of hierarchically structured materials, flower-like materials have been proved to be favorable to the entry of visible light and to

enhance light scattering.[30,31] Inspired by the previous work, herein we design dual-chamber MFCs equipped with flower-like CIS photocathode.

In this study, we investigated photocatalysis on the cathode
5 reaction by using flower-like CIS photocathode as an alternative catalyst comparing with Pt. Furthermore, it has been reported that CIS displayed light harvesting properties in visible-light region,[26] indicating the feasibility of CIS for visible-light-activated photocatalytic application. Linear sweep voltammetry (LSV) and
10 photocurrent tests were employed to confirm the photoelectrochemical property of CIS, meanwhile cyclic voltammetry (CV) to determine the energy levels in solar-assisted MFC (solar MFC). Based on the process of electron transfer, we proposed the hypothesized mechanisms of the solar-assisted
15 electron transfer by flower-like CIS cathode.

2. Experimental section

2.1. Reagents and Materials

Cuprous chloride (CuCl), Indium chloride (InCl$_3$·4H$_2$O), sublimed sulfur and triethylene glycol used in this study were of
20 analytical grade and supplied by Shanghai Chemical Corp. All reagents were used without any purification. Ultrapure water (18 MΩ cm) was used for all experiments.

2.2. Preparation of CuInS$_2$

In a typical synthesis, 1.0 mmol CuCl, 1.0 mmol InCl$_3$·4H$_2$O, and
25 2.5 mmol sublimed sulfur powders were dispersed in 30 mL of triethylene glycol under stirring, and then ultrasonication for 30 min to form a yellow-green suspension. Afterwards, the suspension was transferred into a 50 mL Teflon-lined stainless steel autoclave. The autoclave was sealed and maintained at 200
30 °C for 48 h. After cooling to room temperature naturally, the final dark products were collected by centrifuging the mixture, washed with absolute ethanol and distilled water several times, and then dried under a vacuum at 60 °C overnight for further use.

2.3. Ink and Electrode Preparation for CuInS$_2$ Photocathode

35 The catalyst ink formulation used in MFC tests was as followed: 20 mg of CIS powder was dispersed in 20 mL of a solvent mixture of Nafion (5 wt %) and anhydrous ethanol (1:9, v:v) for 1 h under sonication.[32,33] In comparison experiment, the commercially available catalyst of 20 wt % Pt/C powder was
40 used to prepare a 1 mg mL^{-1} Pt/C suspension by following the same procedure as that detailed above.

For MFC cathode fabrication, the inks were spun onto the Fluorine-doped tin oxide (FTO) glass substrates with an active area of 4 cm^2 and the catalyst loading on the FTO substrate was 1
45 mg cm^{-2}.

2.4. MFC Construction and Operation

All MFC tests were conducted by using a dual-chamber MFC. For the anodic chamber, we used *Shewanella oneidensis* MR-1 (ATCC 70050) as the biocatalyst.[34] *Shewanella ondidensis* MR-1
50 was grown in 100 mL of Tripticase Soy Broth (TSB) under aerobic conditions at 30 °C for 36 h, then centrifuged and resuspended in 1 L of a nutrient medium[35,36] previously purged with nitrogen gas to eliminate oxygen. Lactate (0.02 M) and

fumarate (0.1 M) were added to the medium as an electron donor
55 and acceptor, respectively. After anaerobic incubation at 30 °C for 48 h, the cells were harvested again by centrifugation, resuspended in chamber under anoxic conditions.[37] The anode chamber was filled with enriched *Shewanella oneidensis* MR-1 cells, carbon granules (1-3 mm in diameter), and a nutrient
60 medium containing lactate (0.02 M).

For the MFC set-up, the FTO coated with CIS was used as the cathode (surface area of 4 cm^2). Meanwhile, the catholyte in the cathode chamber was a phosphate buffer solution (PBS) (0.1 M, pH 7.0). In order to maintain oxygen for the electrochemical
65 reaction, oxygen was purged into the cathode compartment. The MFC experiments were carried out in batch mode, configuring as a dual-chambered MFC model, which was composed of the cathode and the anode chamber pressed together with a net volume of 200 mL. The two compartments were separated by a
70 Nafion 117 membrane with 3 cm in diameter. Stainless steel wire and some copper wires were used to connect the circuit. All experiments were performed at room temperature.

2.5. Electrochemical Analysis and Data Acquisition

The photocurrent measurements of CIS were employed using a
75 three-electrode configuration with CIS/FTO or FTO as working electrode, Ag/AgCl (3 M KCl) and a platinum wire serving as the reference and counter electrodes respectively. The working electrode potential and current were controlled by an electrochemical workstation (CHI 660C, Chenhua Instrument
80 Co., China). A Xenon lamp (50 mW cm^{-2}) was used for light irradiation with a filter (λ ≥ 400 nm), and electrolyte was a PBS solution (0.1 M, pH 7.0). In addition, LSV measurements were performed at a scan rate of 10 mV s^{-1} in the dark or under Xenon light illumination with the same three-electrode system. In
85 addition, CV measurement was performed to estimate the oxidation and reduction potential at a scan rate of 50 mV s^{-1}, and tetrabutylammonium perchlorate dissolved in acetonitrile (0.1 M) was used as supporting electrolyte.

Power density ($P = IV/A$) for the MFCs was measured by a
90 SourceMeter (2400 Keithley, Cleveland, OH), according to the measured voltage (V), current ($I = V/R$), and surface area of the photoelectrode (A).The maximum power output was determined by the polarization and power density curves.

2.6. Sample Characterization

95 The crystal structure of the sample was investigated by the wide-angle (10° - 80°, 40 kV/200 mA) powder X-ray diffraction (XRD) measurement with a polycrystalline X-ray diffractometer (RIGAKU, D/MAX 2550 VB/PC, λ = 1.5406 Å). The element composition was characterized by energy dispersive spectra (EDS)
100 with an energy dispersive X-ray analyzer (Falion 60S) and Inductively Coupled Plasma-Atomic Emission Spectrometry (ICP-AES) using an analyzer (IRIS 1000). The morphology of the CIS/FTO cathode was examined by scanning electron microscopy (SEM) using a HITACHI S-4800F microscope.
105 Optical microscope (BX51-OOLYMPUS) was used to observe the growth state of microorganism.

3. Results and discussion

3.1. Characterization of CuInS$_2$

Structure characterization of the CIS microspheres formed on FTO substrate was conducted by XRD (Fig. 1). Fig. 1a presents the pattern of CIS immobolized on FTO substrate (noted as

5   CIS/FTO), and the patterns of FTO (Fig. 1b) and CIS (Fig. 1c) are also illustrated in the figure for comparison. In the XRD pattern of Fig. 1c, the peaks at 27.8°, 32.2°, 46.3°, 55.0° and 74.7° can be indexed to (112), (004), (204)/(220), (116)/(312) and (316) crystal planes of chalcopyrite CIS (JCPDS card No.85-

10   1575), respectively. FTO substrate shows three typical diffraction peaks at 26.5°, 38° and 51.5°, respectively, which is the typical X-ray diffraction peaks of FTO, and this is corresponding to the previous report.[38] The result suggested pure CIS was obtained by employing solvothermal method.
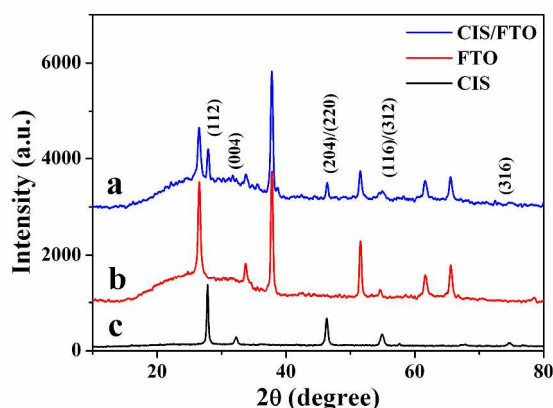

15

Fig. 1. XRD pattern of (a) as-prepared CIS product, (b) the bare FTO substrate, (c) CIS on FTO.

The morphology of the CIS microspheres was examined by SEM (Fig. 2). Fig. 2A displayed the panoramic image of CIS,

20   revealing that the sample consists of spherical flower-like hierarchitectures with an average diameter of about 3 μm. Fig. 2B exhibited the high-magnification SEM image of CIS hierarchical microsphere. It can be noted that the flower-like microspheres are built by many interleaving packed two-dimensional flakes. The

25   mechanism for the formation of CIS was proposed as follow, the involved CuS microspheres form in situ and then act as the self-sacrificed templates, resulting in the flower-like CIS.[26] Hierarchically porous structure enabled CIS microspheres with the ability to enhance light harvesting, which makes CIS as an

30   effective photocatalyst for solar-assisted applications.[18,26,29]

According to EDS and ICP-AES measurements, we obtained information about the elemental compositions of as-synthesized flower-like CIS microspheres. Fig. 3 showed a typical EDS spectrum, which confirmed the existence of Cu, In, and S

35   elements in as prepared CIS sample. The elemental compositions of as prepared CIS were also determined by EDS and ICP-AES, and the results were shown in Table 1. Furthermore, the stoichiometric composition in EDS spectrum results in a Cu:In:S ratio of 1:1.14:2.16 whereas ICP-AES measurements gave a

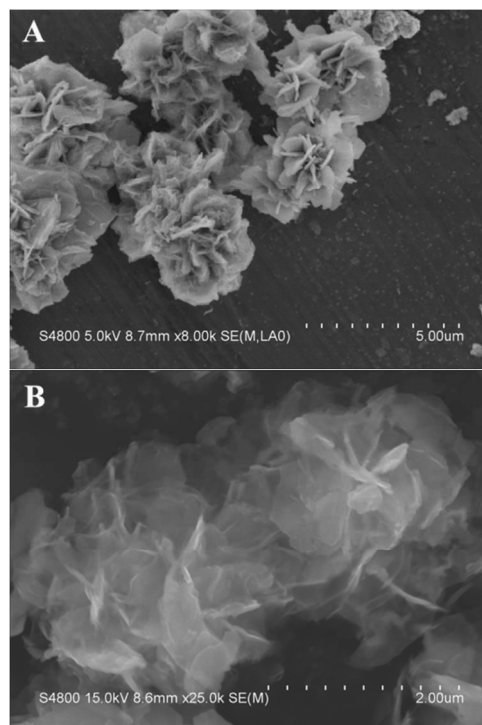40   Cu:In:S ratio of 1:1.05:1.94. The two methods displayed consistent results with the components.

Fig. 2. Representative SEM images of CIS microspheres (A) low-
45 magnification image of CIS; (B) high-magnification SEM image of flower-like CIS.
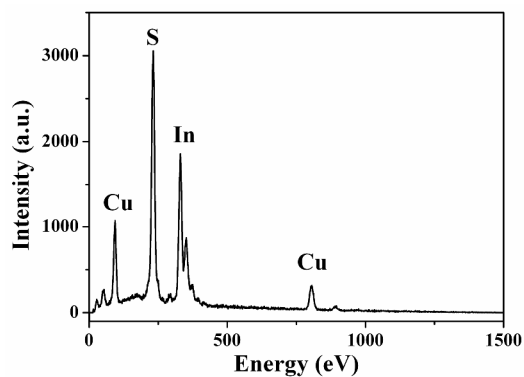

Fig. 3. A typical EDS spectra of CIS.

Table 1. Stoichiometry of CIS sample, obtained by EDS and ICP-AES
50 analysis.

Test method	Cu	In	S
EDS	1	1.14	2.16
ICP-AES	1	1.05	1.94

3.2. Electrochemical property of CuInS$_2$

To confirm the mechanism of electron transfer between bioanode and photocathode, we measured the redox potential of CIS using CV electrochemical behavior, which has been proven to be an
55 effective method for the determination of energy levels. From CV spectra, the band edge positions (i.e., the highest occupied molecular orbital (HOMO) and lowest unoccupied molecular orbital (LUMO) energy position) can be determined. Oxidation potential was correlated with the ionization potential (I_p) and the
60 reduction potential with the electron affinity (E_a), the band edge positions of electroactive materials can be calculated.[39] The HOMO and LUMO energy levels can be derived from the onset

oxidation potential (E_{ox}) and onset reduction potential (E_{red}), respectively, according to equations below:[40]

$$E_{HOMO} = -I_p = -(E_{ox} + 4.72) \text{ eV} \qquad (1)$$
$$E_{LUMO} = -E_a = -(E_{red} + 4.72) \text{ eV} \qquad (2)$$

5 where the onset of potential values are relative to a Ag/AgCl reference electrode. The value of 4.72 represents the vacuum level potential of the normal hydrogen electrode (NHE) (i.e., 0 V *vs.* NHE ≈ 4.5 eV *vs.* vacuum) and the potential of the Ag/AgCl electrode versus NHE (0 V *vs.* Ag/AgCl ≈ 0.22 V *vs.* NHE).[40]

10 Fig. 4 exhibited an oxidation onset of CIS at ca. 1.07 V and a reduction onset at ca. -0.76 V *vs.* Ag/AgCl reference electrode, which are measured based on the previous report.[36] According to equation (1) and (2), the HOMO and LUMO levels of CIS can be calculated as -5.8 eV and -4.0 eV, respectively. The oxidation and 15 reduction potentials of CIS *vs.* NHE can be calculated as 1.29 V and -0.54 V, respectively. The VB of semiconductor is corresponding to HOMO energy level (oxidation onset), while CB is corresponding to LUMO level (reduction onset). To receive microbial electrons, the semiconductor should have a VB edge 20 more positive than the electrochemical potentials of bacterial outer membrane c-type cytochrome (Omc) proteins (*e.g., Shewanella* cell have reported -0.1 V *vs.* NHE).[41] To reduce protons generated at the bioanode, the semiconductor should have a CB edge more negative than ORR at neutral pH (0.82 V *vs.* 25 NHE).[18] According to the above principles of electron transferring, the energy positions of CIS could be benificial for ORR in solar MFC. The details of energy levels would be displayed in the description of the scheme of solar MFC.
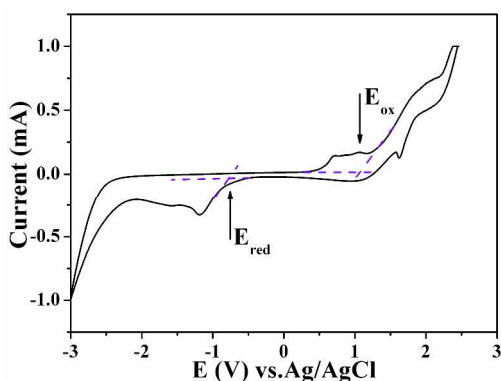

30 **Fig. 4.** CV measurement for the prepared CIS.

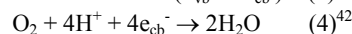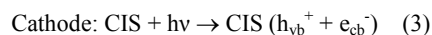### 3.3. Hypothesized Mechanisms of Photocatalytic Electron Transfer

In an MFC, the cathode carries the electrocatalyst for facilitating transfer of electrons generated from the anode to electron 35 acceptor in electrolyte, thus to achieve the electrical circuit. In the dark, CIS catalysis is presumed similar to other catalyst such as Pt. Upon light illumination, electron-hole separation is obtained at the surface of CIS cathode. The photogenerated electrons from CB of CIS (e_{cb}^-) can reduce the electron acceptors in electrolyte 40 (such as dissolved O_2) at the cathode-electrolyte interface, while the photogenerated holes in the VB (h_{vb}^+) recombine with the electrons generated at bioanode to form electric circle.[19] In this study, the dual chamber MFC equipped with flower-like CIS photocathode shows improved performance than plain cathode 45 MFC, implying the significance of light assistant effect of light-

responsive semiconductors on MFC systems. Owing to the photogenerated electron-hole pairs of CIS under visible light irradiation, the electons generated by bacteria on the anode might be driven by the photogenerated holes to transfer more efficiently 50 to the cathode, where the oxygen reduction reaction happened.[21] The whole process could be depicted with equations below and
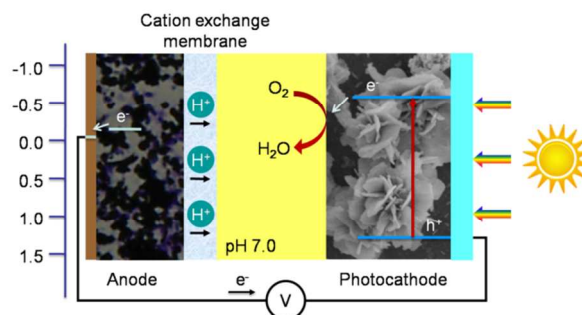
Scheme 1. Energy diagram illustrates the charge transfer process between a microbial anode and a CIS cathode working under visible light irradiation.

55 summarized in Scheme 1.

$$\text{Cathode: CIS} + h\nu \rightarrow \text{CIS} (h_{vb}^+ + e_{cb}^-) \qquad (3)$$
$$O_2 + 4H^+ + 4e_{cb}^- \rightarrow 2H_2O \qquad (4)^{[42]}$$

3.4. Photo-response of CuInS$_2$

To evaluate the mechanism of solar-assisted CIS cathode, we 60 collected LSV curves and amperometric I-*t* plots with a light illumination of 50 mW cm^{-2} (Fig. 5). Fig. 5A showed LSV curves recorded from CIS/FTO and FTO for comparison. The dark scan of CIS/FTO (black solid line) led to a small current density at 0.1
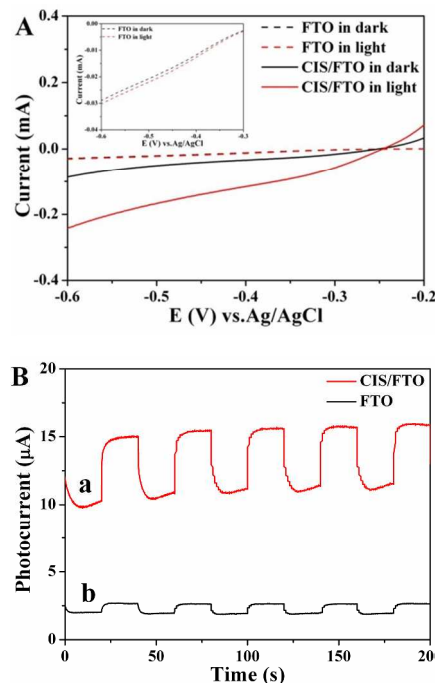

65 **Fig. 5.** (A) LSV curves collected from CIS/FTO and FTO with scan rate of 10 mV s^{-1} in dark and at Xenon lamp illumination (50 mW cm^{-2}, λ ≥ 400 nm) in 0.1 M pH 7.0 PBS, respectively; Inset: comparison of FTO in dark and light illumination (B) Photocurrent responses of (a) CIS/FTO, 70 (b) FTO under Xenon lamp illumination in 0.1 M pH 7.0 PBS

mA, while under illumination the CIS/FTO exhibited photocurrent density up to 0.25 mA (red solid line) at a bias of -0.6 V *vs*. Ag/AgCl. The photocurrent suggested efficient light absorption of CIS and charge separation at the semiconductor/catholyte interface.[21]The inset of Fig.5A showed the magnified photocurrent of FTO substrates under dark and light irradiation. From the inset of Fig. 5A, it could be seen that the photocurrent of FTO substrate in light condition is about 0.03 mA, which is slightly higher than that of in dark. Amperometric I-*t* curve (Fig. 5B) collected at appropriate voltage of -0.2 V *vs*. Ag/AgCl with light on-off cycles showed that the CIS photocathode had reproducible photocurrent generation in response to light illumination of 50 mW cm^{-2} (curve b). Taken together, the LSV curves and photocurrent data demonstrated that photogenerated electron-hole pairs can be driven by solar light, which indicated CIS could be beneficial for electron transfer with improved electricity generation.

3.5. MFC Performance of CuInS$_2$ Photocathode

Fig. 6A displayed the growth state of *Shewanella* as anode of MFC: well dispersed and hard combined with graphite particles. Polarization tests were investigated to evaluate the utility of CIS as a photocathode in MFC. Fig. 6B presented the polarization curves and power density of MFCs. Table 2 summarized main parameters obtained from MFC tests. As shown in Fig. 6 and Table 2, there were (1) a MFC using a CIS photocathode at a solar light illumination of 50 mW cm^{-2} (red solid line); (2) a MFC using plain FTO photocathode (black solid line); (3) Pt/C as cathode in MFC (blue solid line). The open circuit voltage (V_{oc}) of 0.53 V and short-circuit current density (I_{sc}) of 0.62 mA cm^{-2} were achieved in CIS photocathode, while 0.46 V and 0.33 mA cm^{-2} corresponding to the bare FTO, respectively. Equipped with CIS photocathode, the MFC device exhibited maximum power density (P_{max}) of 0.108 mW cm^{-2}, which was two times higher compared with plain FTO (0.047 mW cm^{-2}). For comparison, Pt/C cathode (I_{sc}=0.72 mA cm^{-2} and P_{max}=0.123 mW cm^{-2}) was slightly higher than CIS as photocathode. These results suggested that flower-like CIS as photocathode can be efficient and comparable to commercial Pt/C catalyst. In addition, the curves in Fig. 5C displayed the performance of MFC with light switching on-off. It can be observed the current density of CIS/FTO in light (red solid line) presented significant increase than CIS/FTO in dark (black solid line). The enhancement confirmed the electron-hole pairs separations at photocathode of CIS were facilitated to release the holes for electrons from bioanode, meanwhile electrons for ORR in cathode, thus improved the electricity generation of MFC. According to the above results, CIS as photocathode presented good power density comparable with Pt/C in MFC. This could be attributed to: the fabricated CIS sample with flower-flake and monodispersity may be beneficial to electron transfer under irradiation thus exhibited enhanced visible-light photocatalytic activity. Based on great advantage of hierarchical architecture, MFCs containing CIS or other semiconductor-coated cathode may offer an effective way for simultaneous electricity production.
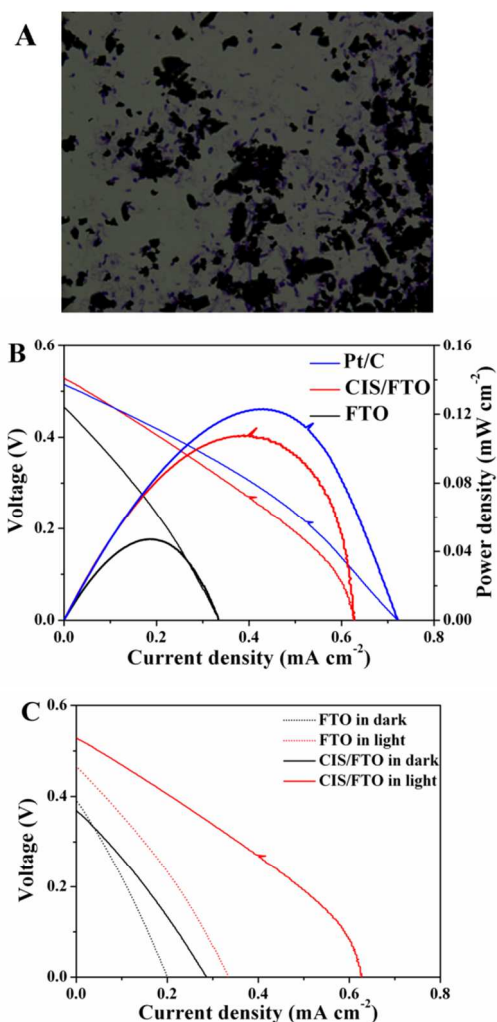

Fig. 6. (A) The optical microscope image of *Shewanella* growing around graphite particles; (B) Representative polarization (thin line) and power density (bold line) curves for MFCs equipped with CIS photocathode (red curve) or plain FTO (black curve) obtained in light illumination, comparison with Pt/C (blue curve) as cathode in dark condition; Inset: polarization curves obtained from CIS/FTO and FTO in dark and light irradiation.

Table 2. Parameters of MFCs with different cathodes.

Sample	I_{sc} (mA cm^{-2})	V_{oc} (V)	P_{max} (mW cm^{-2})
FTO	0.33	0.46	0.047
CIS/FTO	0.62	0.53	0.108
Pt/C	0.72	0.51	0.123

4. Conclusions

In summary, we have demonstrated that the flower-like CIS microspheres could be used as a cathode material for solar MFC. Hierarchical structure makes CIS as an effective photocatalyst for solar-assisted applications. The flower-like CIS shows enhanced photocurrent generation under visible light irradiation, and reveals that CIS could be beneficial for electron transfer with enhanced electricity production. The polarization curve and power density tests confirm its feasibility with CIS as photocathode. The current density, open circuit voltage and

maximum power density of up to 0.62 mA cm^{-2}, 0.53 V and 0.108 mW cm^{-2} have achieved in a simple MFC device without any chemical surface modification. The power density is close to commercial Pt/C catalyst. Based on this study, further and
5 systematic investigations are required to fully exploit the potential of this class of photocathode materials.

Acknowledgements

Notes and references

*Key Laboratory for Ultrafine Materials of Ministry of Education, School
15 of Materials Science and Engineering, East China University of Science and Technology, Shanghai 200237, China. E-mail: xlyang@ecust.edu.cn; yhzhu@ecust.edu.cn; Fax: +86 21 6425 0624; Tel: +86 21 6425 2022*

1. K. Rabaey and W.Verstraete,*Trends Biotechnol,* 2005, **23**, 291–298.
2. B. E. Logan, B. Hamelers, R. Rozendal , U. Schroder, J. Keller, S.
20 Freguia, P. Aelterman, W. Verstraete and K. Rabaey*, Environ. Sci. Technol., 2006, 40, 5181–5192.*
3. D. R. Lovely, *Curr. Opin. Biotechnol.*, 2006, **17**, 327–332.
4. F. Zhao, R. C. T.Slade and J. R.Varcoe, *Chem. Soc. Rev.*, 2009, **38**,1926–1939.
25 5. J. J. Fornero, M. Rosenbaum, M. A. Cotta and L. T. Angenent, *Environ. Sci. Technol.*, 2008, **42** ,8578–8584.
6. Q. Deng, X. Y. Li, J. N. Zuo, A. Ling and B. E. Logan, *J. Power Sources*, 2010, **195**, 1130–1135.
7. B. H. Kim, I. S. Chang and G. M. Gadd, *Appl. Microbiol. Biotechnol.,*
30 2007, **76**, 485–494.
8. X. W. Liu, X. F. Sun, Y. X. Huang, G. P. Sheng, S. G. Wang and H. Q. Yu, *Energy Environ. Sci.*, 2011, **4**, 1422–1427.
9. S. J. You, Q. L. Zhao, J. N. Zhang, J. Q. Jiang, C. L. Wan, M. A. Du and S. Q. Zhao,. *J. Power Sources*, 2007, **173**, 172–177.
35 10. K. Y. Cheng, G. Ho and R. Cord-Ruwisch, *Environ. Sci. Technol.*, 2010, **44**, 518–525.
11. S. Freguia, K. Rabaey, Z. Yuan and J. Keller, *Electrochim. Acta,* 2007, **53**, 598–603.
12. S.A. Cheng, H. Liu and B. E. Logan, *Environ. Sci. Technol.*, 2006,
40 **40** ,364–369.
13. H. J. Hou, L. Li, P. D. Figueiredo and A. Hana, *Biosens. Bioelectron.*, 2011, **26**, 2680–2684.
14. H. Liu, S. Grot and B. E. Logan, *Environ. Sci. Technol.*, 2005, **39**, 4317–4320.
45 15. C. H. Feng, Q. Y. Wan, Z. S. Lv, X. J. Yue, Y. F. Chen and C. H. Wei, *Biosens. Bioelectron.*, 2011, **26**, 3953–3957.
16. X. W. Liu, X. F. Sun, Y. X. Huang, G. P. Sheng, K. Zhou, R. J. Zeng, F. Dong, S. G. Wang, A. W. Xu, Z. H. Tong and H. Q. Yu, *Water Res.,* 2010, **44**, 5298–5305.
50 17. Y. Yuan, B. Zhao, Y. Jeon, S. K. Zhong, S. G. Zhou and S. Kim, *Bioresour. Technol.*, 2011, **102**, 5849–5854.
18. X. W. Liu, W. W. Li and H. Q.,Yu, *Chem. Soc. Rev.* ,2014, DOI: 10.1039/c3cs60130g.

19. H. Lu, Y. Li, S. Jin, H. Ding, C. Zeng, X. Wang and C. Wang,
55 *Energy Fuels,* 2009, **24**, 1184–1190.
20. Q. Y. Chen, J. S. Liu, Y. Liu and Y. H. Wang, *J. Power Sources*, 2013, **238**, 345-349.
21. F. Qian, G. M. Wang and Y.Li, Nano Lett., 2010, **10**, 4686–4691.
22. Q. P.Chen, J. H. Li, X. J. Li, K. Huang, B. X. Zhou, W. M. Cai and
60 W. F. Shangguan, *Environ. Sci. Technol.*, 2012, **46**, 11451−11458.
23. Z. Zhang, R. Dua, L.B. Zhang, H.B. Zhu, H. N. Zhang, P. Wang, *ACS Nano*, 2013, **7**, 1709–1717.
24. X. Sheng, L. Wang, L. T. Chang, Y. P. Luo, H. Zhang, J. Z. Wang and D. R. Yang, *Chem. Commun.*, 2012, **48**, 4746-4748.
65 25. J. H. Yun, Y. H. Ng, S. J. Huang, G. Conibeer and R. Amal, *Chem. Commun.*, 2011, **47**, 11288-11290.
26. L. Zheng, Y. Xu, Y. Song, C. Z. Wu, M. Zhang and Y. Xie, *Inorg. Chem.*, 2009, **48**, 4003-4009.
27. S. Y. Liu, J. J. Hu and X. G. Su, *Analyst*, 2012, **137**, 4598-4604.
70 28. S. Y. Liu, H. Zhang, Y. Qiao and X. G. Su, *RSC Adv.*, 2012, **2**, 819-825.
29. Y. Li, Z. Y. Fu and B. L. Su, *Adv. Funct. Mater.* 2012, **22**, 4634-4667.
30. H. X. Li, Z. F. Bian, J. Zhu, D. Q, Zhang, G. S. Li, Y. N. Huo, H. Li and Y. F. Lu, *J. Am. Chem. Soc.*, 2007, **129**, 8406-8407.
75 31. Y. N. Huo, J. Zhang, M. Miao and Y. Jin,. Appl. Catal. B: Environ., 2011, **111-112**, 334-341.
32. R. Liu, D. Wu, X. Feng and K. Müllen, *Angew. Chem. Int. Ed.*, 2010, **49**, 2565-2569.
33. Z. S. Wu, S. Yang, Y. Sun, K. Parvez, X. Feng and K. Müllen, *J. Am.*
80 *Chem. Soc.*, 2012, **134**, 9082-9085.
34. Y. H. Su, Y. H. Zhu, X. L. Yang, J. H. Shen, J. D. Lu, X. Y. Zhang, J. D. Chen and C. Z. Li, *Ind. Eng. Chem. Res.,* 2013, **52**, 6076−6082.
35. D. R. Lovley and E. J. Phillips, *Appl. Environ. Microbiol.*, 1988, **54**,1472-1480.
85 36. J. R. Kim, B. Min and B. E. Logan, *Appl. Microbiol. Biotechnol.* 2005, **68**, 23-30.
37. N. Uria, X. Munoz Berbel, O. Sanchez, F. X. Munoz and J. Mas, *Environ. Sci. Technol.,* 2011, **45**, 10250-10256.
38. M. L. Sun, W. Y. Fu, Q. Li, G. C. Yin, K. L. Chi, J. W. Ma, L.H.
90 Yang, Y. N. Mu, Y. L. Chen, S. Su, W. J. Zhang and H.B. Yang, *RSC Adv.*, 2014, **4**, 7178–7184.
39. S. H. Chang, M. Y. Chiang, C. C. Chiang, F. W. Yuan, C. Y. Chen, B. C. Chiu, T. L. Kao, C. H. Lai, and H. Y. Tuan, *Energy Environ. Sci.,* **2011**, 4, 4929-4932.
95 40. W. J. Yue, S. K. Han, R. X. Peng, W. Shen, H. W. Geng, F. Wu, S. W. Tao and M. T. Wang, *J. Mater. Chem.,* 2010, **20**, 7570–7578.
41. E. Marsili, D. B. Baron, I. D. Shikhare, D. Coursolle, J. A. Gralnick and D. R. Bond, *Proc. Natl. Acad. Sci. U.S.A.*, 2008, **105**, 3968–3973.
100 42. H. Y. Wang, F. Qian, G. M. Wang, Y. Q. Jiao, Z. He and Y. Li, *ACS Nano*, 2013, **10**, 8728-8735.